RJC

RASĀYAN *J. Chem.*
Vol. 17 | No. 3 |875-896| July - September | 2024
ISSN: 0974-1496 | e-ISSN: 0976-0083 | CODEN: RJCABP
http://www.rasayanjournal.com
http://www.rasayanjournal.co.in

STRUCTURAL BASIS OF NOVEL ANTI-ROSACEA ACTIVE AGENT THROUGH INHIBITION OF KLK5 AND LL-37 GENE EXPRESSION: *In-silico* MODULATION

D. Hikmawati[1], T. M. Fakih[2,3,✉], E. Sutedja[4], R. F. Dwiyana[4] and N. Atik[5]

[1]Department of Dermatology, Faculty of Medicine, Universitas Islam Bandung, Bandung, Indonesia, 40116

[2]Department of Pharmacy, Faculty of Mathematics and Natural Sciences, Universitas Islam Bandung, Bandung, Indonesia, 40116

[3]Department of Pharmaceutical Analysis and Medicinal Chemistry, Faculty of Pharmacy, Universitas Padjadjaran, Sumedang, Indonesia, 45363

[4]Department of Dermatology and Venereology, Faculty of Medicine, Universitas Padjadjaran-Dr. Hasan Sadikin Hospital, Bandung, Indonesia, 40161

[5]Department of Biomedical Sciences, Faculty of Medicine, Universitas Padjadjaran, Sumedang, Indonesia, 45363

✉Corresponding Author: taufikmuhammadf@unisba.ac.id

ABSTRACT

Rosacea is a skin condition characterized by inflammation, and efforts to develop its treatment are ongoing. Overactivation of the enzymes Kallikrein-5 (KLK5) and peptide Cathelicidin (LL-37) has been identified as a regulatory factor in rosacea. Excessive activation of KLK5 and LL-37 can lead to chronic inflammation and manifest in symptoms like facial redness, swelling, and the formation of pustules. These molecules are crucial in the inflammatory process and can compromise the skin's integrity. Our study aimed to identify potential compounds from the ZINC20 database for rosacea therapy using virtual screening guided by *in-silico* molecular docking studies, *in-silico* molecular dynamics simulations, and *in-silico* protein-peptide molecular docking studies targeting KLK5 and LL-37. Initially, we optimized the geometries of selected compounds from the ZINC20 database and then performed molecular docking studies and molecular dynamics simulations on KLK5, as well as protein-peptide molecular docking studies on LL-37. During drug similarity analysis of the compounds, we observed no violations of Lipinski's five rules and found no evidence of hepatotoxicity. Based on the docking score for KLK5, we identified ZINC compounds with favorable molecular interactions. Subsequently, we conducted 200 ns MD simulations and assessed system stability using RMSD, RMSF, Rg, H-bonding, RDF, SASA, and MM-PBSA. Among the ZINC compounds, ZINC000022339916 demonstrated superior stability compared to others, as well as azelaic acid and native ligands. Moreover, ZINC000888090135 and ZINC000888088617 were capable of preventing LL-37 from binding to the surface of KLK5. These findings highlight the potential of these compounds in inhibiting KLK5 activity and disrupting LL-37 interactions in the context of rosacea treatment.

Keywords: ZINC Compounds, Kallikrein-5, Cathelicidin, Rosacea Therapy, Computational Study.

RASĀYAN *J. Chem.*, Vol. 17, No.3, 2024

INTRODUCTION

There have been many recent studies in early 2022 regarding the potential of developing new therapies for rosacea with the Kallikrein-5 (KLK5) pathway inhibition.[1,2] One of them, a study conducted by Hikmawati et al stated that compounds with the codes ZINC000409414675, ZINC000888088617, ZINC000888090135, ZINC000001893410, ZINC000022339916, and ZINC000012444335 have a good affinity compared to azelaic acid as a comparison.[3] Nevertheless, further research needs to be carried out to confirm the mechanism of the reaction pathway in Cathelicidin (LL-37) inhibition.[4,5]

KLK5 and LL-37 are interconnected in the pathogenesis of rosacea. Excessive KLK5 activity can cause damage to the skin barrier and stimulate the production of LL-37, an antimicrobial peptide involved in the immune response in the skin.[6] Increased production of LL-37 caused by excessive KLK5 activity can trigger inflammation and cause redness of the skin. LL-37 can also increase the production of IL-1, which is a pro-

inflammatory cytokine that exacerbates inflammation in rosacea. In addition, LL-37 can also trigger an adaptive immune response that exacerbates rosacea.[7,8]

Therefore, inhibition of KLK5 and LL-37 has been identified as a potential target for the development of new therapies for rosacea.[9] Inhibition of both can have some positive effects on skin conditions affected by rosacea. KLK5 inhibition may help prevent damage to the skin barrier and decrease LL-37 production.[10] This can help reduce the inflammation and redness of the skin associated with rosacea. KLK5 can also break down collagen and elastin, proteins that help maintain skin strength and elasticity.[11,12] Inhibiting KLK5 is expected to significantly contribute to the development of future skin care therapies.[13]

New research for the discovery of KLK5 and LL-37 inhibitor therapy is needed because rosacea therapy is still limited so far. Although there are several medications available to treat rosacea symptoms, such as topical medications containing metronidazole or azelaic acid, these medications only help temporarily reduce symptoms and do not completely cure the condition.[14] Hence, an *in-silico* modulation will be planned for the development of more effective and safer therapies to treat rosacea, which could provide significant benefits for rosacea sufferers.[15]

EXPERIMENTAL

Kallikrein-5 (KLK5) Receptor Preparation

The receptor protein's three-dimensional (3D) arrangement is obtained by downloading a file in the PDB format from the Research Collaboratory for Structural Bioinformatics Protein Data Bank (RCSB PDB) website. The PDB ID codes used for Kallikrein-5 (KLK5) are 2PSX[16] and 6QFE (chain A)[17] respectively. To improve the structure of the receptor protein, Chimera software version 1.17 was used which was the creation of this resource originates from the Resource for Biocomputing, Visualization, and Informatics at the University of California San Francisco, located in San Francisco, CA, USA.[18] The structure of the receptor protein is then optimized through an energy minimization process by performing 1000 steps of steepest descent using an average squared gradient of 0.02 Å with the application of the Amber ff14SB-ILDN force field. The accuracy of the chemical spatial configuration of the receptor protein structure was confirmed through the utilization of PROCHECK, specifically examining the Ramachandran plot.[19] The Ramachandran plot of the modeled receptor protein shows that 92% of the residues are within the region of interest, followed by 8% within the additional allowable region, indicating a model of good quality.

Binding Site Kallikrein-5 (KLK5) Receptor Prediction

The acronym CAST-p (http://sts.bioe.uic.edu/castp/index.html?201l) refers to the Computed Atlas of Surface Topography of Proteins, which functions as a web server.[20] The chief aim of CAST-p is to forecast the size, surface area, and geometry of active regions within proteins, which are probable sites for ligand binding. In this study, the server was employed to identify the specific locations and surface areas of active sites for all the protein targets under investigation. In order to employ the CAST-p server effectively, protein targets were submitted in the PDB format, and the probe radius was established at the standard value of 1.4 angstroms. The information obtained from this analysis proved crucial in ensuring the accuracy of subsequent docking procedures.

ZINC Compound Preparation

Six compounds derived from the ZINC20 database (https://zinc20.docking.org/) namely ZINC000409414675, ZINC000888088617, ZINC000888090135, ZINC000001893410, ZINC000022339916, and ZINC000012444335, together with azelaic acid as a comparison, was used as a ligand in studies on KLK5.[3] The construction and rectification of the ligand's three-dimensional structure were executed through GaussView 6.1.1 and Gaussian16 software employing the Density Functional Theory (DFT) technique utilizing Becke's potential functional theory, employing the 3-parameter, Lee-Yang-Parr (B3LYP) approach with a 3-21G basis set.[21] To ensure the stability of the structure, the vibration frequency is calculated using the same theoretical method. Improved ligand structures and partial loading data were used as inputs in molecular docking studies.

Drug-Likeness Properties of the Zinc Compound

The drug-like characteristics of all compounds were evaluated utilizing the SwissADME server, necessitating the input of canonical Simplified Molecular Input Line Entry System (SMILES)

representations.[22] The evaluation was based on Lipinski's rule of five (Ro5), which considered four key parameters. Firstly, the molecular weight (MW) had to be less than or equal to 500 g/mol. Secondly, the consensus log p-value (log p) had to be less than or equal to 5, indicating appropriate lipophilicity. Thirdly, the number of hydrogen bond donors (HBD) should not exceed five. Fourthly, the number of hydrogen bond acceptors (HBA) needed to be less than or equal to ten. It is important to note that passing these parameters does not guarantee oral activity of the compounds. Hence, supplementary parameters indicative of drug-likeness were considered, including ensuring that the topological polar surface area (TPSA) remained at or below 140 $Å^2$, and the count of rotatable bonds (RB) did not exceed ten. These additional parameters provide better estimates of the compounds' likelihood of being pharmacologically active. To evaluate the safety profile of the compounds, their potential for causing irritation, mutagenicity, tumorigenicity, and reproductive effects was assessed utilizing the OSIRIS software acquired from the organic chemistry portal.[23] This step is crucial in understanding the potential adverse effects and safety considerations of the compounds, making it an integral part of the drug discovery and development process.

In-Silico Molecular Docking Study

For the virtual molecular docking screening, AutoDock 4.2, sourced from MGLTools 1.5.7 (https://ccsb.scripps.edu/mgltools/), was employed with its default configurations.[24] The ligand exhibiting the top docking score is regarded as the most stable conformation among those associated with the receptor protein. Six compounds from the ZINC20 database, azelaic acid, and native ligands were selected for further analysis. Preparation is carried out on the ligands by adjusting the twistable bonds and adding a Gasteiger charge. The water molecules in the KLK5 crystal structure were removed manually from the PDB files before the molecular docking process, and polar hydrogen was added. The docking process specific to the KLK5 binding site was carried out using native ligands to obtain the binding pocket. This pocket is formed with a lattice size of 64 × 60 × 60 and a spacing of 0.375 Å, spanning all known native ligand-binding sites. The structure of KLK5 and the ligand was converted into PDBQT format, and the docking procedure was adjusted to maintain the flexibility of the ligand and the rigidity of the protein. Electrostatic and affinity mapping for all types of atoms is calculated. During the docking procedure, the Lamarckian genetic algorithm (GA 4.2) is employed, conducting 100 random conformation searches and enforcing a maximum evaluation cap of 2,500,000. The crystallized ligands in the 2PSX and 6QFE (chain A) structures were used as validation to check the accuracy of the protocol, and the root mean square deviation (RMSD) value was calculated. Among these modes, the top two binding modes, characterized by the highest molecular docking scores and interactions with the specified receptor proteins, were preserved as PDB files for subsequent analysis. The interactions between receptor proteins and ligands were visualized using the Discovery Studio Visualizer v.2021, available for free download from https://discover.3ds.com/discovery-studio-visualizer-download.[25] The conformation with the lowest energy level was selected as the input for the molecular dynamics simulation.

In-Silico Molecular Dynamics Simulations

To verify the outcomes of molecular docking, molecular dynamics (MD) simulations were conducted on the protein-ligand complex. The simulations were performed using GROMACS-2016.3 software, employing a simulation period of 200 nanoseconds and the Amber ff14SB-ILDN force field.[26] The force field parameters for the ligands were generated using the AnteChamber PYthon Parser interfacE (ACPYPE).[27] The TIP3P aqueous model was employed to solvate the complex, followed by the introduction of sodium and chloride ions to achieve neutralization. Periodic boundary conditions (PBC) were implemented, and energy minimization was carried out until it reached a threshold of 1000 kJ/mol/nm. The system was subjected to equilibration in both constant temperature-constant volume (NVT) and constant temperature-constant pressure (NPT) ensembles for a duration of 1 nanosecond. To attain complete charge neutrality and an ionic strength of 0.15 M, a suitable number of Na+ and Cl- ions were added in lieu of solvent molecules. An energy reduction process was initiated at the onset of the simulation to alleviate significant forces and allow system relaxation. The temperature and pressure were kept constant at 310 K and 1.0 bar, respectively, using a Nose-Hoover thermostat and a Berendsen barostat.[28] The trajectories of the simulation were recorded at intervals of 2 femtoseconds and stored every 2 picoseconds. Following the completion of the molecular dynamics (MD) simulation, post-simulation analysis was conducted,

encompassing the computation of root mean squared deviation (RMSD), root mean squared fluctuation (RMSF), radius of gyration (Rg), radial distribution function (RDF), solvent-accessible surface area (SASA), assessment of secondary structure, and analysis of hydrogen bonds.

MM-PBSA Binding Energy Calculation

The g_mmpbsa tool within the GROMACS-2016.3 software package was employed to conduct the Molecular Mechanics Poisson-Boltzmann Surface Area (MM-PBSA) analysis. This analysis is designed to compute the binding affinity and residual energy contributions involved in protein-ligand interactions.[29] The energy computation process comprises three sequential steps: determining the potential energy in a vacuum, calculating the polar solvation energy, and computing the non-polar solvation energy. The electrostatic energy is evaluated by considering the exponential damping factor, employing the Debye-Huckel theory.[30]

This process, termed as MM-PBSA screening, involves utilizing the MmPbSaStat.py script to derive the average binding energy and obtain a summary of energy terms. Furthermore, the MmPbSaDecomp.py script is utilized to determine the average energy contribution of each residue. In solving the linear approximation of the Poisson–Boltzmann (PB) equation, dielectric constants for the solute and solvent were set at 2 and 80, respectively, while the ion strength was established at 150 mM. The apolar energy contribution is assessed utilizing surface area approximations with γ set to 0.0226778 kJmol^{-1} Å^{-2} and β (a fitting parameter) set to 3.84982 kJmol^{-1}. For this analysis, 500 frames from each simulated complex are employed.

***In-Silico* Protein-Peptide Molecular Docking Study**

To assess the inhibitory potential of each ligand Cathelicidin (LL-37) attachment, protein-peptide molecular docking was carried out between LL-37 and the structure of the KLK5 protein complex obtained from the final trajectory of molecular dynamics simulations. The crystal structure of LL-37 was acquired from the Research Collaboratory for Structural Bioinformatics Protein Data Bank (RCSB PDB) (https://www.rcsb.org/) (PDB ID 2K6O) and processed for further analysis.[31] Protein-peptide interactions were analyzed using the PatchDock (http://bioinfo3d.cs.tau.ac.il/PatchDock/) server.[32] The server utilizes the soft molecular surfaces' shape complementarity to generate the optimal initial solution. Grouping was conducted employing the default root mean square deviation (RMSD) with a maximum distance of 2.0 Å, selecting the protein-peptide complex type. PatchDock generates molecular surface representations, including convex, concave, and flat patches, through appropriate algorithms.

The PatchDock solution is then optimized for small-sized molecules, resulting in a list of fixed complexes. In this process, the relative orientation of the molecules is changed by limiting the flexibility of the interacting surface side chains and allowing the movement of small rigid bodies. Re-evaluation was carried out on the top 10 candidate solutions by considering the PatchDock scoring and atomic contact energy (ACE) score. The outcomes of molecular protein-peptide docking were determined according to the scores generated by these methods. To observe interactions and bindings within docked conformations, the Discovery Studio Visualizer v.2021 software is utilized, which can be obtained at no cost from https://discover.3ds.com/discovery-studio-visualizer-download.[25]

RESULTS AND DISCUSSION

Binding Site Kallikrein-5 (KLK5) Receptor Prediction

The surface areas (SA) for the Kallikrein-5 (KLK5) targets with PDB ID 2PSX and 6QFE (chain A) have been estimated to be 152.490 Å and 80.880 Å, respectively. Fig.-1 provides a visual representation of these surface areas in high-resolution 3D output. The surface area measurements are crucial as they offer valuable insights into the extent of the exposed regions on the protein's surface.[33] Understanding the surface area can aid in identifying potential binding sites for ligands or other interacting molecules, which is particularly significant for studying the function and regulation of Kallikrein-5. Additionally, these surface area estimations can serve as valuable input for further computational analyses, such as molecular docking studies, to investigate the interactions of KLK5 with various ligands or inhibitors.[34] Overall, the high-resolution 3D output in Fig.-1 enhances our understanding of the structural features and potential binding sites of the KLK5 targets.

Drug-Likeness Properties of the ZINC Compound

Lipinski's Rule of Five Analysis

The successful validation of Lipinski's rule of five (Ro5) for evaluating drug likeness was confirmed (Table-1). The first criterion, the limit on molecular weight (MW ≤ 500), was satisfied. Among the six best-performing compounds, all of them adhered to Lipinski's parameters, ensuring that their overall molecular weight remained below 500 g/mol. As for medical drugs, the compounds ZINC000409414675, ZINC000888088617, ZINC000888090135, ZINC000001893410, ZINC000022339916, and ZINC000012444335 meet this criterion, as their molecular weights do not exceed the specified limit. The second and third criteria limit the number of hydrogen bond donors (HBD ≤ 5) and acceptors (HBA ≤ 10), respectively, all of which are met by the compounds. Similarly, compounds sourced from the ZINC20 database also adhere to these criteria, with no more than 5 hydrogen bond donors and hydrogen bond acceptors not exceeding the specified maximum limit of 10. The final parameter is the threshold value of log p (log p ≤ 5), which all compounds, including medicinal drugs, remain within.[35] Additionally, all ZINC compounds exhibit positive values, indicating a higher affinity for the lipid phase. While adherence to these five rules does not guarantee absolute drug similarity, it does increase the likelihood of higher oral bioavailability for the compounds.

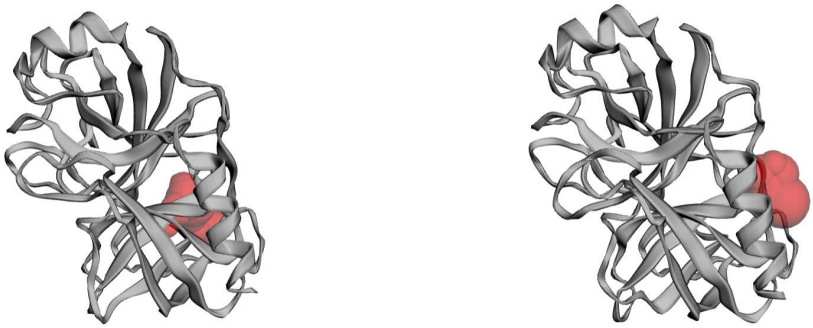

Fig.-1: CAST-p Pocket Estimation: On the left is PDB ID 2PSX, and on the Right is PDB ID 6QFE (chain A)

Two additional parameters for drug similarity, namely the number of twistable bonds (RB ≤ 10) and the TPSA value [(TPSA) ≤ 140 Å^2)], offer more specific insights into potential oral bioavailability. All six compounds fulfill the requirements of both parameters, as they have less than 10 bonds that can be rotated, and their TPSA values are below 140 Å^2.[36] These results align with Lipinski's rule of five, indicating promising oral bioavailability potential. However, compound ZINC000001893410 passed the first parameter but failed the second one due to its significantly higher TPSA value of 190.30 Å^2. Consequently, this particular compound cannot be considered suitable for oral administration. Nevertheless, it is essential to note that failure to meet these parameters does not necessarily imply a lack of drug potency as a whole.[37]

Swiss-ADME Output

The Swiss-ADME parameters provide further insights into the characteristics of the examined compounds (Table-2). The compounds ZINC000409414675, ZINC000001893410, ZINC000022339916, and ZINC000012444335 exhibit moderate solubility, while the compounds ZINC000888088617 and ZINC000888090135 are notably soluble. Out of the six ZINC compounds, five display high bioavailability scores, indicating their potential for effective absorption in the body. However, compound ZINC000001893410 received the lowest score for oral bioavailability, suggesting that it may not be as efficiently absorbed when administered orally. Additionally, all ZINC compounds, except ZINC000001893410, demonstrate high gastrointestinal (GI) absorption, further supporting their potential as viable drug candidates. Fig.-2 displays the hard-boiled egg graphs, illustrating the relationship between TPSA (X-axis) and Log p (Y-axis) for all ZINC compounds. Among the six compounds, only five were observed to undergo passive absorption through the gastrointestinal (GI) tract. Remarkably, only ZINC000001893410 exhibited suitability for gastrointestinal tract absorption, indicating its promising bioavailability.

Table-1: The Drug-Likeness of the Best Compounds was Assessed Based on Lipinski's Criteria as well as Additional Parameters

Compound ID	Chemical Structure	Molecular Weight (g/mol)	Rotatable Bonds	H-Bond Donors	H-Bond Acceptors	C Log p	TPSA (Å^2)
		MW ≤ 500	RB ≤ 10	HBD ≤ 5	HBA ≤ 10	Log p ≤ 5	TPSA ≤ 140
ZINC000409414675	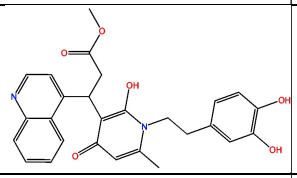	474.51	8	3	7	3.31	121.88
ZINC000888088617	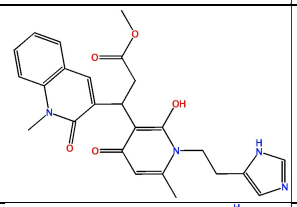	462.50	8	2	6	2.47	119.21
ZINC000001893410	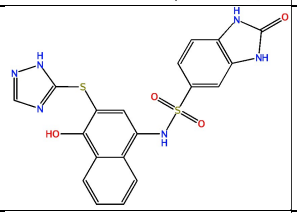	454.48	5	5	6	2.10	190.30
ZINC000888090135	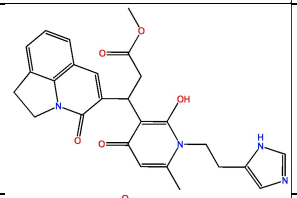	474.51	8	2	6	2.45	119.21
ZINC000022339916	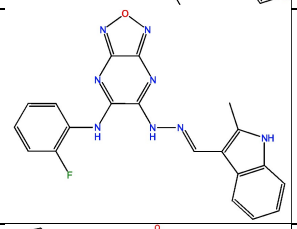	402.38	5	3	7	3.48	116.91
ZINC000012444335	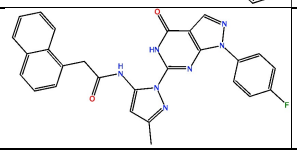	493.49	6	2	6	3.92	110.49

Table-2: The Swiss-ADME Parameters were Selectively Applied to Evaluate the Best Compounds

Compound ID	Chemical Structure	Water Solubility	Bioavailability	GI Absorption	BBB Permeant
ZINC000409414675	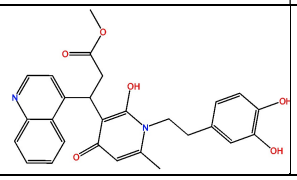	Moderately soluble	0.55	High	No

ZINC000888088617	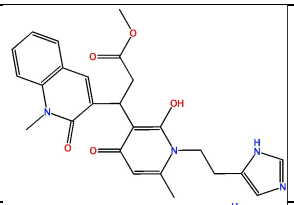	Soluble	0.55	High	No
ZINC000001893410	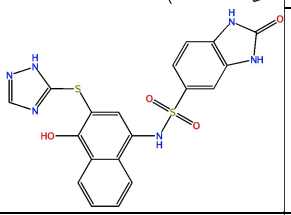	Moderately soluble	0.55	Low	No
ZINC000888090135	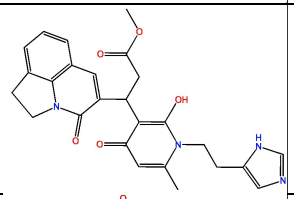	Soluble	0.55	High	No
ZINC000022339916	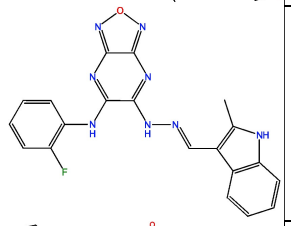	Moderately soluble	0.55	High	No
ZINC000012444335	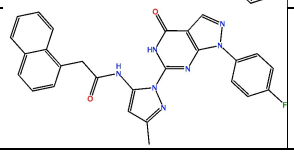	Moderately soluble	0.55	High	No

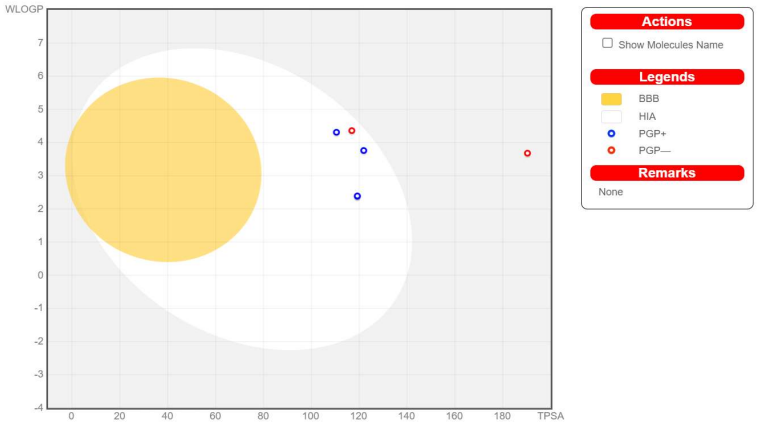

Fig.-2: The Swiss-ADME Boiled Egg Graph Illustrates the Permeability of all ZINC Compounds

OSIRIS Analysis

The OSIRIS analysis provides information regarding possible adverse effects of these compounds, include mutagenicity, tumorigenicity, irritability, and their potential impact on the reproductive system (Table-3). This analysis is crucial in evaluating the safety profile of the compounds and identifying any potential risks associated with their use. It helps researchers and drug developers make informed decisions about the suitability and further development of these compounds for pharmaceutical applications. The OSIRIS analysis concluded that all ZINC compounds carry low risks based on a comprehensive evaluation of factors such as C log p, log s, molecular weight, risk of toxicity, and drug similarity.[38] As a result, the six ZINC

compounds were considered to be potentially treatable. This assessment provides valuable guidance for researchers and pharmaceutical experts to prioritize and explore these compounds further for potential therapeutic applications with minimized risks of adverse effects.

Table-3: The OSIRIS Output Provides Information Regarding Potential Harmful Properties and the Druggability of the Best Compounds

Compound ID	Chemical Structure	Irritant Potential	Mutagenic Potential	Tumorigenic Potential	Reproductive Potential
ZINC000409414675	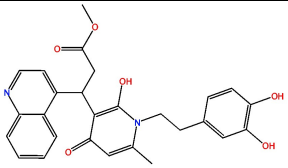	Low	Low	Low	Low
ZINC000888088617	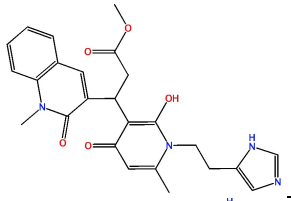	Low	Low	Low	Low
ZINC000001893410	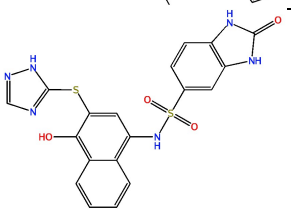	Low	Low	Low	Low
ZINC000888090135	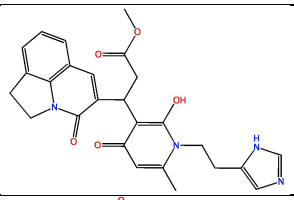	Low	Low	Low	Low
ZINC000022339916	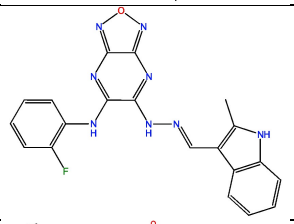	Low	Low	Low	Low
ZINC000012444335	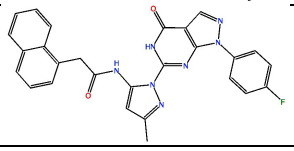	Low	Low	Low	Low

In-silico Molecular Docking Study

Proteins and ligands are optimized to achieve a state of minimum energy, promoting greater stability for the molecules. The stability is reached when the energy of the molecules is reduced to a lower level.[39] Fig.-3 demonstrates the forecast of the ligand-binding site of the target protein using the hydrophobic surface model. In this research, AutoDock 4.2 from MGLTools 1.5.7 was employed to evaluate the ligand docking and protein targeting of Kallikrein-5 (KLK5), ligands with the lowest free energy values (measured in kcal/mol) within the high-affinity binding site are considered. High-affinity ligands have the potential to induce conformational changes in the substrate, thus impacting its functionality. The structures exhibiting the highest binding affinities predominantly involve significant interactions through hydrogen bonding.[40] Table-4 reveals various interactions, most of which are observed between amino acids and ligands. The interactions encompass hydrogen bonds (depicted in green), alkyl and pi-alkyl interactions (in pink), pi

cations (in orange), pi-sulfur interactions (in yellow), Van der Waals interactions (in light green), halogen bonds (in blue), and carbon-hydrogen bonds (in grey).

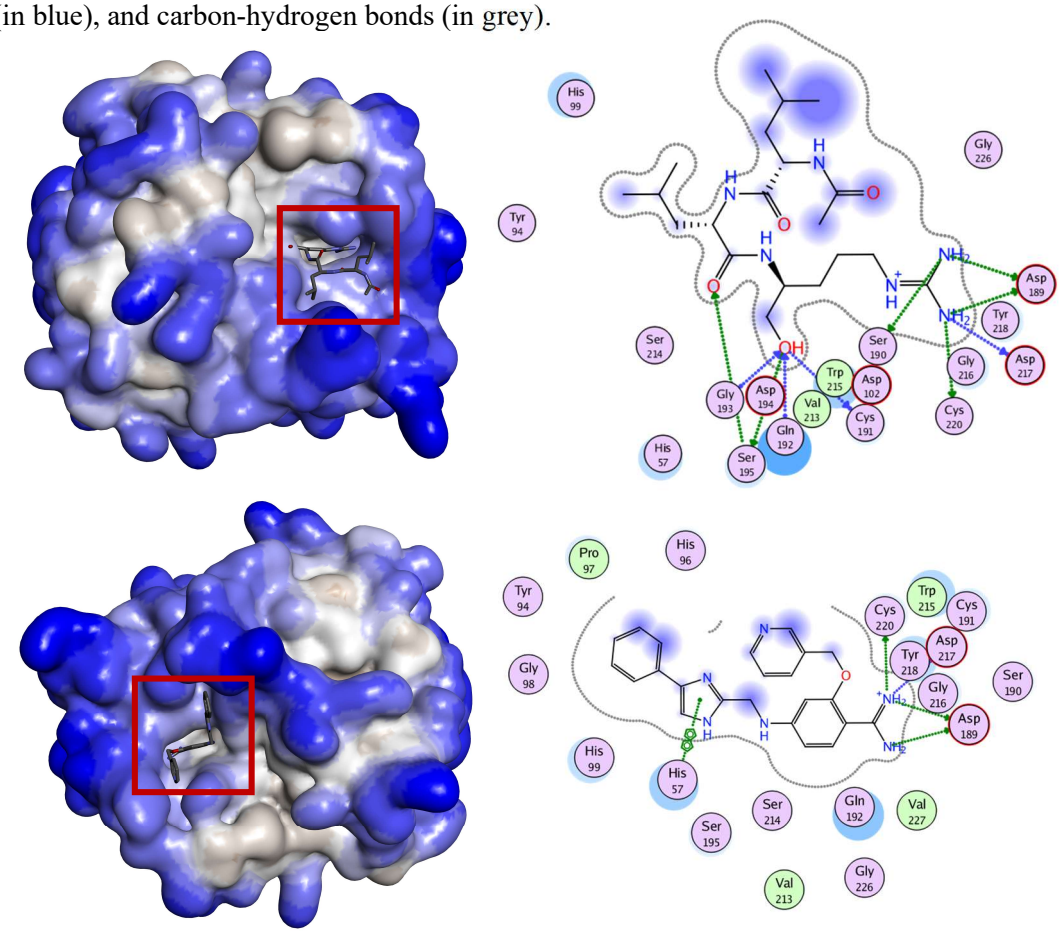

Fig.-3: Forecasted Ligand-Binding Regions are Depicted for Two Protein Structures: On the Top is PDB ID 2PSX, and on the Bottom is PDB ID 6QFE (chain A)

Kallikrein-5 (KLK5) Targets with PDB ID 2PSX

Kallikrein-5 (KLK5) plays a crucial role in specific biological functions, including the kallikrein cascade, which is involved in processing and activating various zymogens and regulating associated signaling pathways. Researchers have investigated KLK5 as a potential target for developing therapeutics and drugs that can modulate its activity, particularly in addressing conditions or diseases like skin inflammation, dermatitis, or other skin-related issues. Understanding KLK5 better and its impact on diverse biological processes could pave the way for more effective and specialized medical interventions to tackle skin-related health concerns and other ailments.[2] In terms of molecular interactions, residues ASP189, SER190, CYS191, GLY193, SER195, ASP217, CYS220, and GLY226 participate in hydrogen bonding, involving Conventional Hydrogen Bonds and Carbon-Hydrogen Bonds. On the other hand, HIS57, HIS99, and TRP215 engage in hydrophobic interactions, displaying Pi-Sigma, and Pi-Alkyl interactions.

Compounds ZINC000022339916 and ZINC000012444335 demonstrated significantly lower docking scores in the KLK5 catalytic pocket, indicating strong binding to KLK5 with binding energies of −6.79 kcal/mol and −9.06 kcal/mol, respectively (Table-4). This robust binding to KLK5 has been verified through AutoDock 4.2 analysis, making these compounds highly effective as potential inhibitors to regulate the excessive or uncontrolled activity of the enzyme. Our computational studies additionally demonstrated that all the examined structures displayed advantageous binding energies towards the target protein, ranging from −6.79 to −9.64 kcal/mol. This range of values was superior to both the native ligand and azelaic acid, suggesting the potential of these compounds to emerge as promising contenders for subsequent drug development endeavors targeting KLK5. Of particular interest, compound ZINC000022339916 exhibited

an intriguing electrostatic interaction with TRP215 and CYS220 residues, forming a Pi-Anion interaction, which may play a crucial role in its binding affinity to KLK5.

Table-4: The Compounds are Identified by Their Respective Compound IDs (first column), and Their Interactions with Kallikrein-5 (KLK5) PDB ID 2PSX are Color-Coded for Better Visualization

Compound ID	Binding Energy (kcal/mol)	Hydrogen Bond	Hydrophobic Interaction	Electrostatic Interaction	Ligand Interaction
Native Ligand	−5.66	ASP189 SER190 CYS191 GLY193 SER195 ASP217 CYS220 GLY226	HIS57 HIS99 TRP215	–	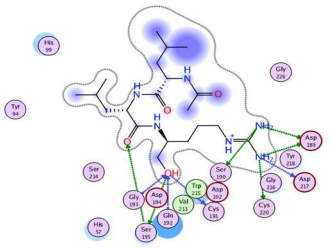
Azelaic Acid	−3.67	GLY193 ASP194 SER195 ASP217 CYS220	–	–	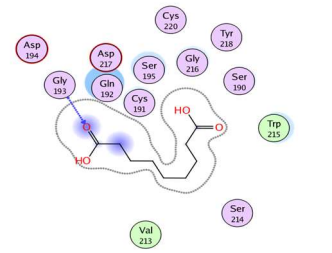
ZINC0004094 14675	−6.79	PRO97 HIS99 ASP189 SER190 GLY216	CYS220	ASP217	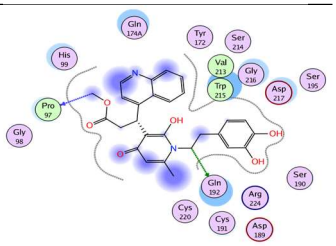
ZINC0008880 88617	−7.39	GLY216 ASP217 GLN174	HIS99 TRP215 CYS220	–	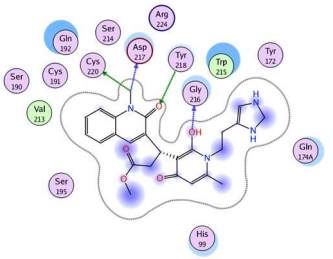
ZINC0000018 93410	−8.08	GLY193 SER195 GLY216	TRP215 CYS220	–	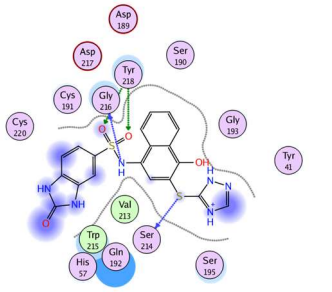

ZINC000888090135	−8.36	GLN192 GLY193 SER195 GLY216	HIS99 VAL213 TRP215 GLY216 ASP217 CYS220 TYR228	–	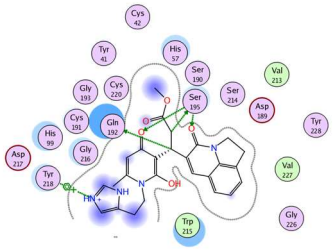
ZINC000022339916	−9.64	GLN174 SER195 GLY216	ASP217	TRP215 CYS220	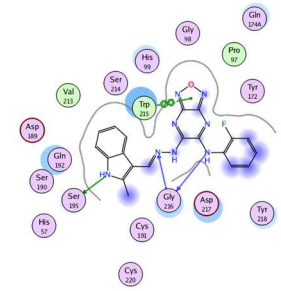
ZINC000012444335	−9.06	GLN192 SER195 GLY216	VAL21 TRP2153	–	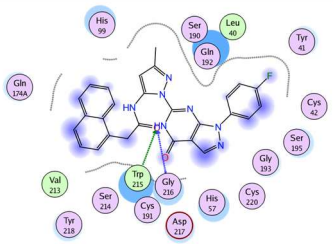

Kallikrein-5 (KLK5) Targets with PDB ID 6QFE (chain A)

The binding active site of KLK5 PDB ID 6QFE (chain A) shows similarities to KLK5 PDB ID 2PSX. Several residues participate in hydrogen bonding interactions, including ASP189, SER190, SER195, SER214, ASP217, CYS220, and GLY226. These interactions involve both Conventional Hydrogen Bonding and Carbon-Hydrogen Bonding. Furthermore, hydrophobic interactions are observed involving HIS57, TRP215, and GLY216, specifically identified as Pi-Pi Stacked and Amide-Pi Stacked interactions. The resemblance in the binding active site and the interactions observed in both KLK5 structures (PDB ID 2PSX and PDB ID 6QFE) holds potential significance for drug design and the targeting of this enzyme in various conditions or diseases where KLK5 plays a role. Further investigation and understanding of these interactions can contribute to the development of therapeutic strategies and drugs that specifically target KLK5 for medical applications.

The data in Table-5 highlights three compounds: ZINC000001893410, ZINC000022339916, and ZINC000012444335. These compounds exhibited notably lower docking scores in the KLK5 catalytic pocket, indicating a strong binding affinity to KLK5, with binding energies of −8.80 kcal/mol, 8.79 kcal/mol, and −9.64 kcal/mol, respectively. The robust binding to KLK5 was validated through AutoDock 4.2 analysis, suggesting that these compounds have the potential to serve as potent inhibitors, capable of regulating excessive or uncontrolled enzyme activity. Moreover, our computational analyses unveiled that all scrutinized structures exhibited favorable binding energies with the target protein, ranging from −7.51 to −9.64 kcal/mol. This range of values surpassed those of the native ligand and azelaic acid, highlighting the promising potential of these compounds for further drug development, specifically targeted at KLK5.

***In-silico* Molecular Dynamics Simulations**

The findings in Table-4 and Table-5 demonstrate that the most effective inhibitors form strong hydrogen bonds and engage in numerous non-covalent interactions. To assess the stability of the protein and investigate conformational changes in the ligand-protein complex, Molecular dynamics (MD) simulations were conducted for a duration of 200 ns.

Table-5: The Compounds are Identified by their Respective Compound IDs (first column), and their Interactions with Kallikrein-5 (KLK5) PDB ID 6QFE (chain A) are Color-Coded for Better Visualization

Compound ID	Binding Energy (kcal/mol)	Hydrogen Bond	Hydrophobic Interaction	Electrostatic Interaction	Ligand Interaction
Native Ligand	−7.90	ASP189 SER190 SER195 TRP215 CYS220 GLY226	HIS57 SER190 CYS191 TRP215 GLY216 CYS220	–	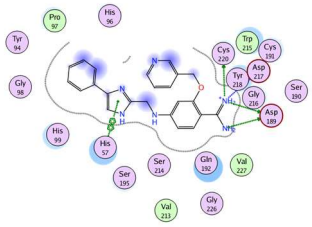
Azelaic Acid	−3.31	SER195 GLY216	–	–	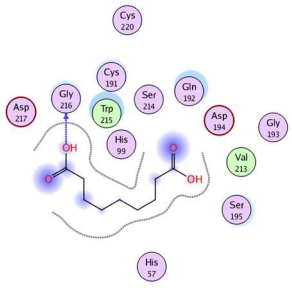
ZINC000409414675	−8.21	ASP102 GLN192 SER214	HIS57 HIS99 CYS191 GLN192 VAL213 TRP215 GLY216 CYS220	–	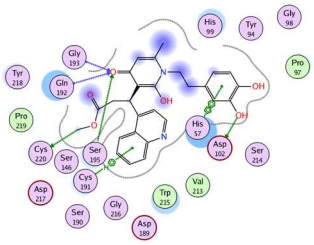
ZINC000888088617	−7.51	SER146 SER195 SER214 GLY216 ASP217	HIS99 CYS191 GLN192 VAL213 TRP215 GLY216 CYS220	–	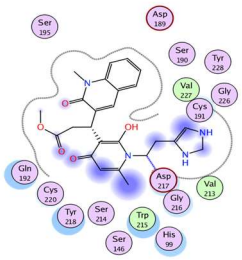
ZINC000001893410	−8.80	GLN192 GLY193 SER195	TYR218 CYS191 GLN192 TRP215 GLY216 CYS220	–	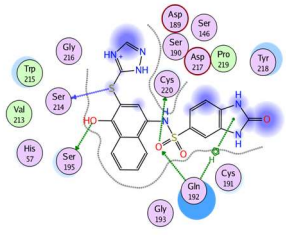
ZINC000888090135	−8.36	GLN174 GLY216	SER190 CYS191 GLN192 VAL213 CYS220	–	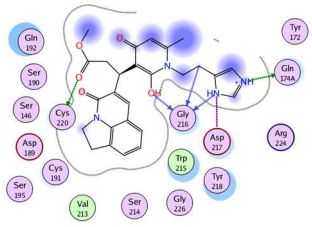

ZINC000022339916	−8.79	SER195 ASP217	CYS42 HIS57 CYS191 GLN192 SER214 TRP215 CYS220	–	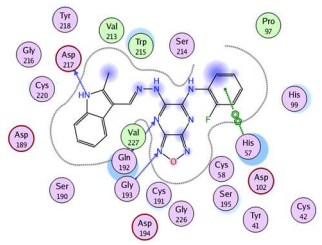
ZINC000012444335	−9.64	GLY193 SER195	HIS57 HIS99 TRP215 GLY216 ASP217 TYR218 CYS220	–	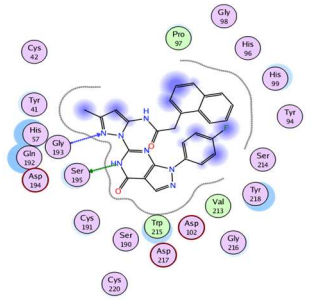

Throughout these molecular dynamics (MD) simulations, trajectory files were meticulously scrutinized, concentrating on diverse parameters such as root mean squared deviation (RMSD), root mean squared fluctuation (RMSF), radius of gyration (Rg), radial distribution function (RDF), solvent-accessible surface area (SASA), secondary structure, and hydrogen bond occupancy. These analyses contribute significantly to the exploration of structural stability and dynamics throughout the MD simulations.[41] All these analyses were vital in investigating the structural stability and dynamic behavior of the ligand-protein complex during the 200 ns MD simulations. The results obtained from these analyses offer valuable knowledge about the behavior and potential stability of the protein-ligand interaction over time, guiding further optimization and development of the identified inhibitors for potential therapeutic applications.

Structural Dynamics of Kallikrein-5 (KLK5) with PDB ID 2PSX

Kallikrein-5 (KLK5) is a crucial factor involved in the regulation of diverse biological processes, with a particular focus on maintaining skin health. As a member of the kallikrein enzyme family, KLK5 serves a vital role in controlling signaling pathways, processing proteins, and activating zymogens. Its primary function lies in breaking down skin proteins, such as profilaggrin and involucrin, into smaller fragments. This enzymatic activity facilitates the shedding of dead skin cells and facilitates the generation of new skin cells, which are essential for upholding skin health and overall integrity.[10] Beyond its role in skin cell turnover, KLK5 also plays a pivotal part in responding to inflammation, balancing the immune system of the skin, and upholding the skin's barrier function. However, when KLK5 activity becomes imbalanced or excessive, it has been linked to various skin disorders, including dermatitis, and other inflammatory skin conditions. Proper regulation of KLK5 is crucial for maintaining healthy skin and preventing skin-related health issues.[4]

RMSD is employed to measure the disparity between the initial and concluding positions of a protein, with a lower RMSD value signifying a more stable structure.[42] The average RMSD values for some of the ZINC compound complexes exhibit a range that is not significantly large, with the lowest value observed in the KLK5-ZINC000888090135 complex at approximately ±0.15 nm (Table-6). These values remained consistently low and stable throughout the simulation, indicating strong and enduring binding between the ZINC compounds and KLK5, effectively blocking its activity. RMSF, on the other hand, describes the fluctuations in residue levels. The RMSF plot reveals that the residues HIS57, HIS99, ASP189, SER190, CYS191, GLY193, SER195, TRP215, ASP217, CYS220, and GLY226, which interact with the KLK5 active site, display higher RMSF values (Fig.-4B), indicating lower stability of these residues overtime during the simulation. The radius of gyration (Rg) indicates the compactness or cohesion of the protein. The average Rg values for each complex do not significantly differ, with the lowest values observed in compounds ZINC000888090135, ZINC000022339916, and ZINC000012444335. These findings suggest that these compounds exhibit significantly stronger binding capability to KLK5 compared to the others. In

this study, protein-native ligand and protein-azelaic acid were used as controls for comparison. RDF is employed in molecular simulations to comprehend the spatial relationships between particles in a system. Similar to the previous analysis, the RDF values do not show substantial differences, with compound ZINC000409414675 having the lowest RDF value of approximately ±3.36 g(r). SASA, or surface area solvent accessible, denotes the extent to of a protein's surface interacts with its surrounding solvent molecules. The best average SASA values were observed in compounds ZINC000409414675 and ZINC000012444335, with SASA values of approximately ±111.83 Å^2 and ±111.81 Å^2, respectively. The plot depicts an increase in the total SASA of the KLK5 complex, indicating that internal residues in KLK5 become more accessible to the solvent when the ZINC compound binds to it (Fig.-4E).

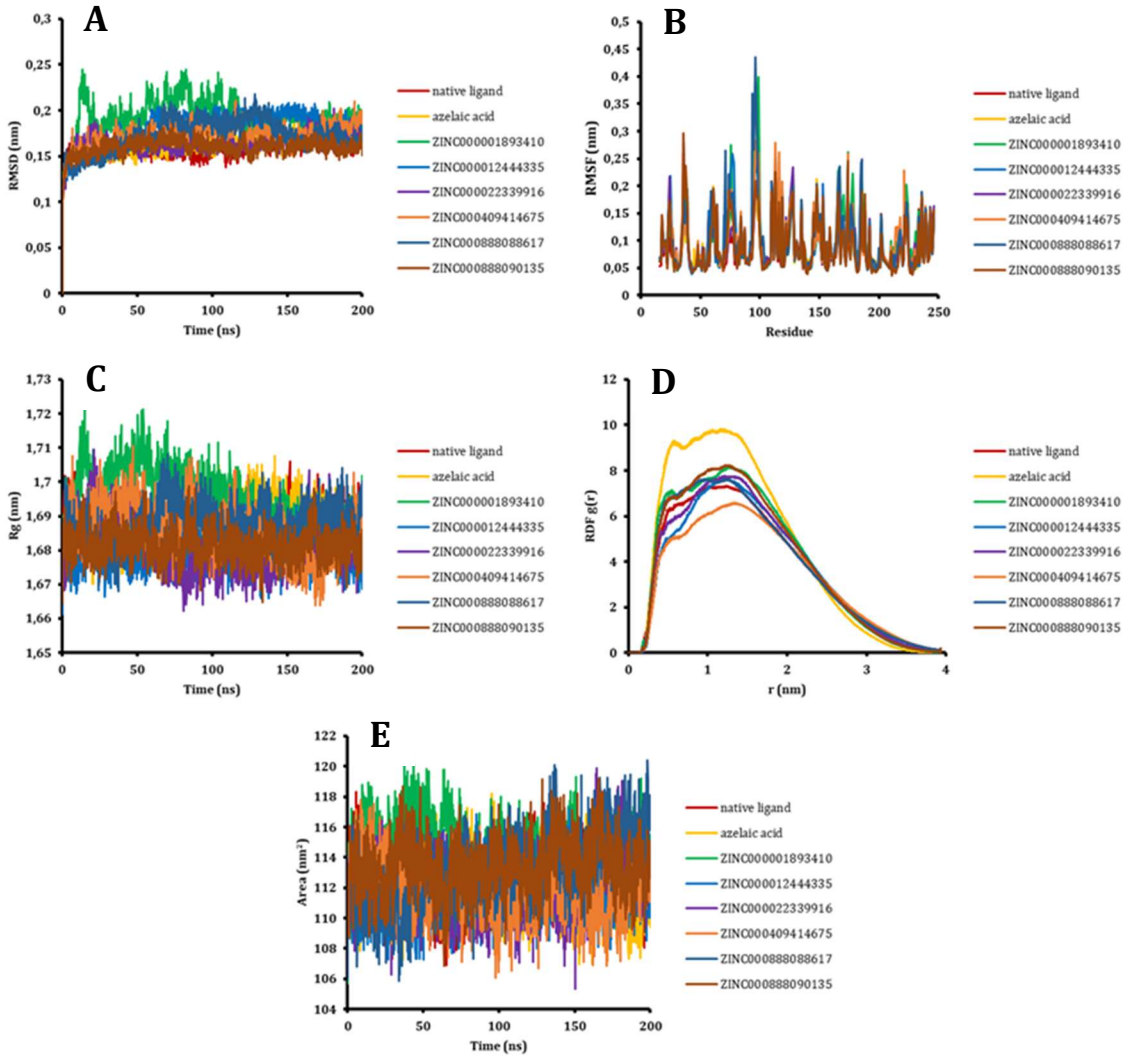

Fig.-4: Structural Dynamics of KLK5 with PDB ID 2PSX. (A) Root Mean Square Deviation (RMSD), (B) Root Mean Square Fluctuations (RMSF), (C) Radius of Gyration (Rg), (D) Radial Distribution Function (RDF), and (E) Solvent-Accessible Surface Area (SASA) Plot

Table-6: The Average Values of RMSD, RMSF, Rg, RDF, and SASA for Kallikrein-5 (KLK5) were Computed Over the 200 ns Duration of the Molecular Dynamics (MD) Simulations

Complex Ligand-Protein	Average RMSD (nm)	Average RMSF (nm)	Average Rg (nm)	Average RDF (g(r))	Average SASA (nm^2)
Native Ligand + KLK5 2PSX	±0.16	±0.09	±1.69	±3.68	±112.50
Azelaic Acid + KLK5 2PSX	±0.16	±0.09	±1.69	±4.49	±112.16

ZINC000409414675 + KLK5 2PSX	±0.17	±0.10	±1.69	±3.36	±111.83
ZINC000888088617 + KLK5 2PSX	±0.17	±0.10	±1.69	±3.78	±113.23
ZINC000001893410 + KLK5 2PSX	±0.19	±0.10	±1.70	±3.97	±114.42
ZINC000888090135 + KLK5 2PSX	±0.15	±0.09	±1.68	±3.94	±113.40
ZINC000022339916 + KLK5 2PSX	±0.16	±0.09	±1.68	±3.73	±112.09
ZINC000012444335 + KLK5 2PSX	±0.18	±0.10	±1.68	±3.62	±111.81
Native Ligand + KLK5 6QFE (chain A)	±0.16	±0.09	±1.69	±4.12	±113.26
Azelaic Acid + KLK5 6QFE (chain A)	±0.16	±0.09	±1.70	±3.69	±112.87
ZINC000409414675 + KLK5 6QFE (chain A)	±0.15	±0.09	±1.68	±4.11	±112.85
ZINC000888088617 + KLK5 6QFE (chain A)	±0.16	±0.09	±1.68	±3.93	±113.04
ZINC000001893410 + KLK5 6QFE (chain A)	±0.15	±0.09	±1.68	±4.15	±112.66
ZINC000888090135 + KLK5 6QFE (chain A)	±0.17	±0.09	±1.68	±3.76	±113.43
ZINC000022339916 + KLK5 6QFE (chain A)	±0.15	±0.08	±1.69	±4.03	±112.77
ZINC000012444335 + KLK5 6QFE (chain A)	±0.17	±0.09	±1.68	±3.32	±113.69

Structural Dynamics of Kallikrein-5 (KLK5) with PDB ID 6QFE (chain A)

KLK5, a serine-type membrane protease protein, plays a crucial role in the skin's proteolytic system. It serves as a vital element in maintaining the balance of proteolysis and protein degradation within the skin. The proteolytic activity of KLK5 is responsible for breaking down various skin proteins, including profilaggrin and involucrin, into smaller fragments.[8] This process is essential in facilitating the exfoliation of dead skin cells and promoting the regeneration of new skin cells, which ultimately contributes to the overall health and integrity of the skin. Beyond its involvement in skin formation and rejuvenation, KLK5 also plays a significant role in regulating the skin's defense system. It achieves this through its influence on the kallikrein cascade and the activation of bioactive peptides. Additionally, KLK5 participates in responding to skin inflammation and contributes to maintaining the skin's barrier function.[1] The multifaceted role of KLK5 highlights its importance in various aspects of skin health and function. Understanding its mechanisms of action and impact on skin biological processes is crucial for the development of therapies and interventions to address skin-related conditions effectively.

The RMSD track is used to assess the deviation of the protein from the reference structure. The ligand's binding within the receptor's binding pocket fosters the overall conformational stability of the entire macromolecular system. In all simulations, the complex attained equilibrium during the last 50 nanoseconds, as highlighted in Table-6. Notably, the average RMSD value decreased during interactions with ZINC000409414675, ZINC000001893410, and ZINC000022339916 (Fig.-5A). These results suggest that the ZINC compounds exhibit stability within the active pocket of KLK5. A marginal rise in residual fluctuations was observed. The average Rg value for ZINC000022339916 was approximately ±1.69 nm, indicating that this compound has a more compact packing compared to KLK5. The compound ZINC000012444335 demonstrated the lowest RDF value, describing the probability distribution of distances between pairs of these compounds. Regarding SASA, the highest values were observed in ZINC000888088617 (±113.04 nm^2), followed by ZINC000888090135 (±113.43 nm^2), and ZINC000012444335 (±113.69 nm^2). This observation indicates that the protein underwent slight volume expansion with minimal fluctuations throughout the simulation period, as outlined in Table-6.

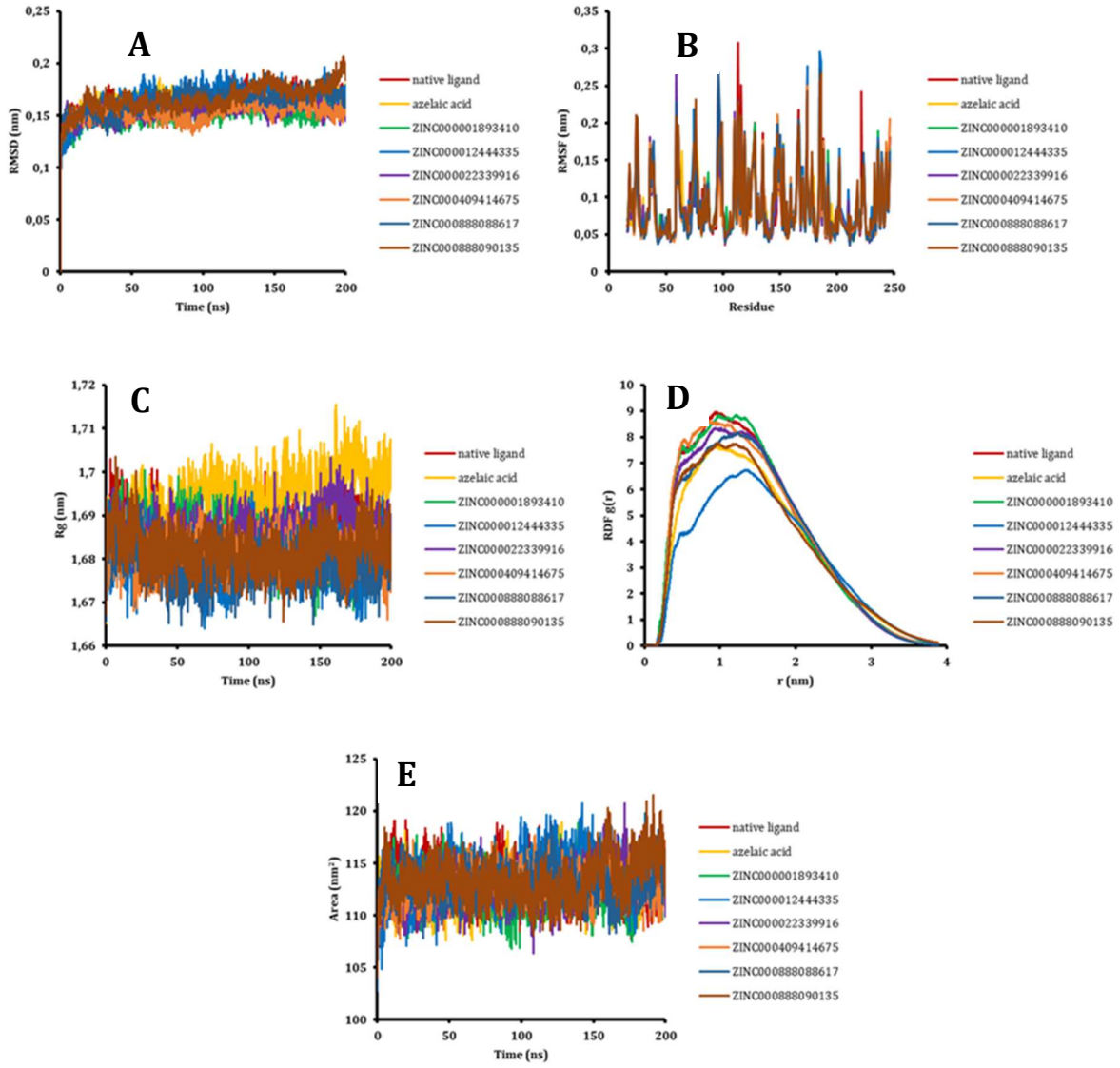

Fig.-5: Structural Dynamics of KLK5 with PDB ID 6QFE (chain A). (A) Root Mean Square Deviation (RMSD), (B) Root Mean Square Fluctuations (RMSF), (C) Radius Of Gyration (Rg), (D) Radial Distribution Function (RDF), And (E) Solvent-Accessible Surface Area (SASA) Plot

Hydrogen Bonding in Molecular Dynamics Simulations

Hydrogen bonds play a pivotal role in maintaining the stability of the protein-inhibitor complex. In evaluating structural stability, hydrogen bonds formed within a cutoff distance of 0.35 nm were scrutinized throughout the 200 ns MD simulation conducted in a solvent environment, as depicted in Table-7.[43] Notably, residues HIS57, HIS99, ASP189, SER190, CYS191, GLY193, SER195, TRP215, ASP217, CYS220, and GLY226 demonstrated significant occupancy, indicating their prominent role in forming hydrogen bonds with KLK5 throughout the simulations. This observation underscores the structural importance of these residues in the KLK5 protein. In the MD simulations, the greatest quantity of hydrogen bonds was observed among the compounds ZINC000888088617, ZINC000001893410, and ZINC000888090135, in the case of KLK5 with PDB ID 2PSX. Subsequently, for KLK5 with PDB ID 6QFE (chain A), the compounds ZINC000001893410 and ZINC000022339916 exhibited the highest number of hydrogen bonds. These results were obtained from two separate sets of MD simulations, each lasting 200 ns. The findings from the hydrogen bond analysis were in line with the tethering approach, although minor disparities were noted in the count of hydrogen bonds between the two methods. This

discrepancy could be attributed to the dynamic nature of ligand-protein interactions and conformational changes that occur during the course of the MD simulations.

Table-7: The Percentage Occupancy of Residue Interactions and Hydrogen Bonds (H-bonds) were Obtained from the Simulation Trajectories

Complex Ligand-Protein	Residue Interaction (H-Bond Occupancy (%))
Native Ligand + KLK5 2PSX	HIS57 (1.20), HIS99 (0.35), ASP189 (0.80), SER190 (3.05), CYS191 (12.39), GLN192 (13.34), GLY193 (1.25), SER195 (24.62), SER214 (14.09), TRP215 (3.45), GLY216 (3.35), ASP217 (7.34), TYR218 (0.05)
Azelaic Acid + KLK5 2PSX	HIS57 (0.05)ASP189 (0.05), GLN192 (3.40), GLY193 (6.20), ASP194 (0.05), SER195 (1.30), GLY196 (0.05), VAL213 (0.05), SER214 (2.40), GLY216 (0.25), ASP217 (4.70)
ZINC000409414675 + KLK5 2PSX	HIS57 (0.10), ASP189 (3.40), SER190 (6.49), GLN192 (5.05), SER195 (0.30), SER214 (0.05), GLY216 (0.50), ASP217 (9.34), TYR218 (0.10)
ZINC000888088617 + KLK5 2PSX	HIS57 (0.10), GLN174 (3.20), GLN192 (11.49), GLY193 (0.05), TRP215 (0.05), GLY216 (2.50), ASP217 (2.95), TYR218 (0.60), ARG224 (0.05)
ZINC000001893410 + KLK5 2PSX	HIS57 (0.10), HIS96 (1.80), HIS99 (0.15), GLN174 (0.45), CYS191 (0.50), GLN192 (31.32), GLY193 (0.15), SER195 (5.35), SER214 (20.03), TRP215 (0.05), GLY216 (8.94), ASP217 (0.70), TYR218 (0.20)
ZINC000888090135 + KLK5 2PSX	TYR41 (15.13), HIS57 (0.95), HIS96 (0.25), HIS99 (0.45), GLN174 (0.15), GLN192 (0.20), GLY193 (0.05), SER195 (43.81), GLY216 (2.75), ASP217 (4.15), TYR218 (0.40)
ZINC000022339916 + KLK5 2PSX	HIS57 (0.10), HIS96 (0.55), HIS99 (0.15), GLN192 (0.10), SER195 (6.89), GLY216 (0.15), TYR218 (0.10)
ZINC000012444335 + KLK5 2PSX	HIS57 (0.45), HIS96 (0.10), GLN192 (30.37), GLY193 (0.10), SER195 (7.04), GLY216 (0.40)
Native Ligand + KLK5 6QFE (chain A)	HIS57 (0.10), ASP189 (22.03), SER190 (61.34), GLY193 (0.20), SER195 (4.80), SER214 (5.24), GLY216 (0.40), ASP217 (0.05)
Azelaic Acid + KLK5 6QFE (chain A)	GLY98 (8.64), HIS99 (0.05), GLN174 (0.05), SER190 (2.85), CYS191 (2.10), GLN192 (1.75), SER195 (0.40), SER214 (1.75), GLY216 (0.85), ASP217 (0.95)
ZINC000409414675 + KLK5 6QFE (chain A)	HIS96 (0.10), GLY98 (0.25), ASP102 (12.74), GLN192 (0.65), SER214 (45.15), GLY216 (1.50)
ZINC000888088617 + KLK5 6QFE (chain A)	TYR41 (1.30), HIS57 (42.36), GLN192 (0.35), SER195 (38.31), GLY216 (0.30), ASP217 (0.05)
ZINC000001893410 + KLK5 6QFE (chain A)	HIS57 (0.65), ARG59 (0.35), GLY98 (1.10), CYS191 (6.79), GLN192 (3.90), GLY193 (2.95), SER195 (48.55), SER214 (0.70), GLY216 (0.80), ASP217 (0.30), TYR218 (0.20)
ZINC000888090135 + KLK5 6QFE (chain A)	GLY98 (0.20), HIS99 (0.55), GLN174 (6.25), GLN192 (0.10), TRP215 (0.40), GLY216 (20.13), ASP217 (0.45)
ZINC000022339916 + KLK5 6QFE (chain A)	TYR41 (0.10), CYS42 (0.05), HIS57 (1.20), ARG59 (0.05), SER190 (0.05), GLN192 (8.14), GLY193 (0.40), SER195 (10.74), GLY216 (0.05), ASP217 (0.70)
ZINC000012444335 + KLK5 6QFE (chain A)	HIS57 (0.60), ARG59 (0.05), SER190 (0.05), GLN192 (0.10), GLY193 (0.40), SER195 (4.70), GLY216 (28.32)

Binding-Free Energy during Molecular Dynamics Simulations

The Molecular Mechanics Poisson-Boltzmann Surface Area method (MM-PBSA) was utilized to improve the precision of predicting the binding free energy of protein-ligand complexes. The computed bond free energies of the complexes are more precise compared to those obtained from the docking studies (Table-8). Significantly, the primary energy contributions stem from electrostatic and van der Waals interactions.[44] Overall, the ZINC compound complexes demonstrated superior stability against KLK5 in the molecular dynamics simulations when compared to the native ligand and azelaic acid. This suggests that the ZINC compounds have favorable binding properties and exhibit strong interactions with KLK5, this suggests their potential as candidates for further exploration as inhibitors or modulators of this enzyme.

Table-8: The Summary Results of MM-PBSA Analysis Provide Valuable Information on the Free Binding Energy and its Individual Components, Making them Relevant for Assessing the Binding Suitability of Molecules to KLK5

Complex Ligand-Protein	ΔE_{vdw} (kJ/mol)	ΔE_{ele} (kJ/mol)	ΔG_{PB} (kJ/mol)	ΔG_{NP} (kJ/mol)	ΔG_{Bind} (kJ/mol)
Native Ligand + KLK5 2PSX	−169.034	−85.767	202.002	−18.744	−71.543
Azelaic Acid + KLK5 2PSX	−104.677	−49.461	125.899	−11.345	−39.585
ZINC000409414675 + KLK5 2PSX	−149.349	−31.658	140.282	−14.215	−54.940
ZINC000888088617 + KLK5 2PSX	−201.120	−35.382	162.490	−18.744	−92.757
ZINC000001893410 + KLK5 2PSX	−178.586	−75.809	178.363	−15.141	−91.174
ZINC000888090135 + KLK5 2PSX	−206.884	−54.657	196.849	−18.767	−83.459
ZINC000022339916 + KLK5 2PSX	−149.088	−255.470	99.501	−14.314	−319.370
ZINC000012444335 + KLK5 2PSX	−151.698	−68.428	144.418	−15.476	−91.183
Native Ligand + KLK5 6QFE (chain A)	−188.362	−78.425	202.183	−17.117	−81.721
Azelaic Acid + KLK5 6QFE (chain A)	−77.876	−47.194	97.479	−9.734	−37.326
ZINC000409414675 + KLK5 6QFE (chain A)	−243.809	−51.847	215.645	−20.373	−100.384
ZINC000888088617 + KLK5 6QFE (chain A)	−197.982	−70.239	188.872	−17.046	−96.396
ZINC000001893410 + KLK5 6QFE (chain A)	−193.521	−89.425	210.439	−16.217	−88.723
ZINC000888090135 + KLK5 6QFE (chain A)	−210.338	−77.517	173.028	−18.130	−132.958
ZINC000022339916 + KLK5 6QFE (chain A)	−183.385	−455.514	224.666	−17.553	−431.786
ZINC000012444335 + KLK5 6QFE (chain A)	−146.286	−34.514	115.051	−13.543	−79.293

Note: ΔE_{vdw} = van der Waals contribution, ΔE_{ele} = electrostatic contribution, ΔG_{PB} = polar contribution of desolvation, ΔG_{NP} = non-polar contribution of desolvation, ΔG_{Bind} = binding-free energy

Of all the ZINC compounds, ZINC000022339916 exhibits the lowest binding free energy during the 200 ns MD simulation, with values of −319.370 kJ/mol (PDB ID 2PSX) and −431.786 kJ/mol (PDB ID 6QFE, chain A). This finding strongly supports the notion that ZINC000022339916 has a highly favorable and stable interaction with KLK5. The significantly low binding free energy indicates strong and robust binding between ZINC000022339916 and the KLK5 protein, making it a promising candidate for further exploration and potential therapeutic development targeting KLK5.

In-silico Protein-Peptide Molecular Docking Study

Protein-peptide docking was conducted to investigate the binding of LL-37 to each component of the KLK5-ligand complex. The binding affinity of LL-37 was assessed using the atomic contact energy (ACE score). The crystal structure of LL-37 was utilized, obtained from the PDB entry with ID 2K6O. To ensure the reliability of the docking method, a method validation step was carried out using PatchDock.[4] This validation process involved the use of a re-docking approach, where LL-37 was docked back into its original crystal structure. The root mean square deviation (RMSD) and active site values were carefully observed during this re-docking process, along with the identification of potential binding residues of LL-37. The results from this method validation phase provided crucial insights into the accuracy and effectiveness of the protein-peptide docking simulation, ensuring the reliability of the subsequent analyses in evaluating the interactions between LL-37 and the KLK5-ligand complex.

Table-9: The Docking Results of the Protein-Peptide Cathelicidin (LL-37) to the KLK5-Ligand Complex

Complex	PatchDock Score	ACE Score (kJ/mol)
Native Ligand + KLK5 2PSX	11070	−256.32
Azelaic Acid + KLK5 2PSX	11680	−401.72
ZINC000409414675 + KLK5 2PSX	12432	−402.39
ZINC000888088617 + KLK5 2PSX	12196	−103.38
ZINC000001893410 + KLK5 2PSX	12202	−41.68
ZINC000888090135 + KLK5 2PSX	11496	85.50
ZINC000022339916 + KLK5 2PSX	12496	−23.34
ZINC000012444335 + KLK5 2PSX	11054	−465.75
Native Ligand + KLK5 6QFE (chain A)	12510	360.10
Azelaic Acid + KLK5 6QFE (chain A)	12652	−521.65
ZINC000409414675 + KLK5 6QFE (chain A)	12300	−503.29
ZINC000888088617 + KLK5 6QFE (chain A)	12202	294.84

ZINC000001893410 + KLK5 6QFE (chain A)	11242	−303.98
ZINC000888090135 + KLK5 6QFE (chain A)	12352	−379.89
ZINC000022339916 + KLK5 6QFE (chain A)	10738	−393.44
ZINC000012444335 + KLK5 6QFE (chain A)	12988	−456.04

Table-9 presents the results of the interaction between the ZINC000888090135 + KLK5 (PDB ID 2PSX) complex and LL-37, indicating a high PatchDock score with ACE and binding energy values of 85.50 kJ/mol each. Conversely, in the KLK5 6QFE (chain A) complex, the ZINC000888088617 compound effectively prevents LL-37 from binding to the surface of KLK5. This observation suggests that ZINC000888090135 + KLK5 (PDB ID 2PSX) complex and KLK5 6QFE complex (chain A) with ZINC000888088617 hold potential as KLK5 inhibitors. The inability of LL-37 to bind to KLK5 in the presence of ZINC000888088617 indicates a potential inhibitory effect on KLK5 activity. These findings offer valuable insights into the promising potential of these compounds as inhibitors of KLK5 and their potential application in the development of therapeutic strategies for conditions or diseases involving KLK5.

Various other conventional Kallikrein-5 (KLK5) inhibitor agents are currently under investigation for potential treatments of different conditions or diseases. However, the available therapeutic options remain limited and suboptimal. Azelaic acid, an FDA-approved compound, has attracted considerable interest owing to its low toxicity and wide-ranging effectiveness in addressing various skin conditions.[45] In the drug similarity analysis of the compounds under scrutiny, no violations of Lipinski's five rules were observed, and there were no indications of hepatotoxicity. This indicates the potential for repurposing and developing derivatives of these ZINC compounds as valuable strategies for future therapeutic interventions. The results of our computational exploration of the tested compounds revealed remarkable to substantial activity against KLK5 target proteins. Among the six ZINC compounds examined, they exhibited superior docking scores compared to the native ligand and azelaic acid.[3]

Hydrogen bonding emerged as the predominant interaction mode with KLK5, being a crucial factor in inhibiting the enzyme's activity. The composition of the ligands indicates the presence of oxygen-containing functional groups, such as ether groups found in ZINC compounds, which offer greater possibilities for enhanced interactions and higher affinity with receptors. Additionally, the presence of a sulfonyl group in certain ZINC derivatives potentially enhances the protein-ligand interaction. The MD simulation analysis affirmed the stability of the assembly, substantiated by RMSD, RMSF, Rg, hydrogen bonding (H-bonding), RDF, and SASA values.[46] These findings offer valuable insights into the potential activity of ZINC compounds and their derivatives as inhibitors of KLK5. Nevertheless, further validation of this target's efficacy against KLK5 requires additional in vitro and in vivo studies. Ensuring that the results from *in-silico* studies can be translated into practical applications is crucial for the development of novel therapies addressing KLK5-related issues.

CONCLUSION

In summary, the computational evaluation of target-specific therapeutic potential aims to narrow down the vast array of derived compounds from the ZINC20 database and identify the most promising candidate for further pharmacological development. Our findings suggest that ZINC compounds hold promise as a novel treatment option against Kallikrein-5 (KLK5). Notably, the results of this *in-silico* study revealed that ZINC000022339916 exhibited superior interactions with KLK5 targets, with MM/PBSA values of −319.370 kJ/mol (PDB ID 2PSX) and −431.786 kJ/mol (PDB ID 6QFE, chain A), indicating its significant potential as an anti-KLK5 agent that warrants further exploration. Additionally, our study demonstrated that compounds ZINC000888090135 and ZINC000888088617 were capable of inhibiting the recruitment of Cathelicidin (LL-37) to the KLK5 surface, as observed in the results of the *in-silico* protein-peptide molecular docking analysis. As a result, the mentioned ZINC compound is currently being procured, and research on its biological activity will be conducted and reported in the near future.

ACKNOWLEDGMENTS

The author expresses gratitude to the Department of Dermatology and Venereology, Faculty of Medicine, Universitas Padjadjaran-Dr. Hasan Sadikin Hospital and Department of Biomedical Sciences, Faculty of Medicine, Universitas Padjadjaran.

CONFLICT OF INTERESTS

The authors declare that there are no conflicts of interest.

AUTHOR CONTRIBUTIONS

All the authors contributed significantly to this manuscript, participated in reviewing/editing, and approved the final draft for publication. The research profile of the authors can be verified from their ORCID IDs, given below:

D. Hikmawati http://orchid.org/0000-0002-1203-5855
T. M. Fakih http://orchid.org/0000-0001-7155-4412
E. Sutedja http://orchid.org/0000-0002-6960-4895
R. F. Dwiyana http://orchid.org/0000-0001-9350-0239
N. Atik http://orchid.org/0000-0001-5951-4733

REFERENCES

1. K. B. Roh, Y. Jang, E. Cho, D. Park, D. H. Kweon, and E. Jung, *Biomedicines*, **10(2),** 463(2022), https://doi.org/10.3390/biomedicines10020463.
2. E. Z. M. da Silva, T. F. de Campos Fraga-Silva,Y. Yuan, M. G. Alves, G. A. Publio, C. K. da Fonseca, M. H. Kodama, G. V. Vieira, M. F. Candido, L. M. A. R. Innocentini, M. G. Miranda, A. R. da Silva, J. C. Alves-Filho,V. L. D. Bonato, R. Iglesias-Bartolome, and K. U. Sales, *Cancers (Basel)*, **13(17),** 4395(2021), https://doi.org/10.3390/cancers13174395.
3. D. Hikmawati, T. M. Fakih, E. Sutedja, R. F. Dwiyana, N. Atik, and D. S. F. Ramadhan, *Informatics in Medicine Unlocked*, **28,** 100844(2022), https://doi.org/10.1016/j.imu.2022.100844.
4. J. Jia, Y. Zheng, W. Wang, Y. Shao, Z. Li, Q. Wang, Y. Wang, and H. Yan, *Molecular Medicine Reports*, **15(1),** 240(2017), https://doi.org/10.3892/mmr.2016.5978.
5. R. Amagai, T. Takahashi, H. Terui, T. Fujimura, K. Yamasaki, S. Aiba, and Y. Asano, *International Journal of Molecular Sciences*, **24(1),** 875(2023), https://doi.org/10.3390/ijms24010875.
6. J. Zhang, P. Jiang, L. Sheng, Y. Liu, Y. Liu, M. Li, M. Tao, L. Hu, X. Wang, Y. Yang, Y. Xu, and W. Liu, *Frontiers in Immunology*, **12,** 609615(2021), https://doi.org/10.3389/fimmu.2021.609615.
7. Y. Matsubara, T. Matsumoto, J. Koseki, A. Kaneko, S. Aiba, and K. Yamasaki, *Molecules*, **22(11),** 1829(2017), https://doi.org/10.3390/molecules22111829.
8. C. Borelli, B. Becker, S. Thude, B. Fehrenbacher, and D. Isermann, *Journal of Cosmetic Dermatology*, **16(4),** e31(2017), https://doi.org/10.1111/jocd.12323.
9. Y. F. Li, X. Y. Chen, and T. C. Lei, *Molecular Medicine Reports*, **18(3),** 2823(2018), https://doi.org/10.3892/mmr.2018.9266.
10. J. B. Lee, S. H. Bae, K. R. Moon, E. Y. Na, S. J. Yun, and S. C. Lee, *Experimental Dermatology*, **25(12),** 956(2016), https://doi.org/10.1111/exd.13133.
11. J. Liddle, V. Beneton, M. Benson, R. Bingham, A. Bouillot A, A. B. Boullay, E. Brook, J. Cryan, A. Denis, E. Edgar, A. Ferrie, M. H. Fouchet, D. Grillot, D. S. Holmes, A. Howes, G. Krysa, A. Laroze, M. Lennon, F. McClure, A. Moquette, E. Nicodeme, B. Santiago, L. Santos, K. J. Smith, J. H. Thorpe, G. Thripp, L. Trottet, A. L. Walker, S. A. Ward, Y. Wang, S. Wilson, A. C. Pearce, and A. Hovnanian, *Journal of Investigative Dermatology*, **141(9),** 2272(2021), https://doi.org/10.1016/j.jid.2021.01.029.
12. J. Kim, M. G. Kim, S. H. Jeong, H. J. Kim, and S. W. Son, *Experimental Dermatology*, **31(2),** 223(2022), https://doi.org/10.1111/exd.14445.
13. Y. Zhu, J. Underwood, D. Macmillan, L. Shariff, R. O'Shaughnessy, J. I. Harper, C. Pickard, P. S. Friedmann, E. Healy, and W. L. Di, *Journal of Allergy and Clinical Immunology*, **140(5),** 1310(2017), https://doi.org/10.1016/j.jaci.2017.01.025.
14. H. Zhang, K. Tang, Y. Wang, R. Fang, and Q. Sun, *Dermatology and Therapy*, **11,** 13(2021), https://doi.org/10.1007/s13555-020-00461-0.

15. A. Li, R. Fang, X. Mao, and Q. Sun, *Photodiagnosis and Photodynamic Therapy*, **38,** 102875(2022), https://doi.org/10.1016/j.pdpdt.2022.102875.
16. M. Debela, V. Magdolen, W. Bode, H. Brandstetter, and P. Goettig, *Biological Chemistry*, **397(12),** 1251(2016), https://doi.org/10.1515/hsz-2016-0205.
17. J. H. Thorpe, E. V. Edgar, K. J. Smith, X. Q. Lewell, M. Rella, G. V. White, O. Polyakova, P. Nassau, A. L. Walker, D. S. Holmes, A. C. Pearce, Y. Wang, J. Liddle, and A. Hovnanian, *Acta Crystallographica Section F:Structural Biology Communications*, **75,** 385(2019), https://doi.org/10.1107/S2053230X19003169.
18. E. F. Pettersen, T. D. Goddard, C. C. Huang, G. S. Couch, D. M. Greenblatt, E. C. Meng, and T. E. Ferrin, *Journal of Computational Chemistry*, **25(13),** 1605(2004), https://doi.org/10.1002/jcc.20084.
19. R. A. Laskowski, M. W. MacArthur, D. S. Moss, and J. M. Thornton, *Journal of Applied Crystallography*, **26(2),** 283(1993), https://doi.org/10.1107/s0021889892009944.
20. W. Tian, C. Chen, X. Lei, J. Zhao, and J. Liang, *Nucleic Acids Research*, **46(W1),** W363(2018), https://doi.org/10.1093/nar/gky473.
21. M. J. Frisch, G. W. Trucks, H. B. Schlegel, G. E. Scuseria, M. A. Robb, J. R. Cheeseman, G. Scalmani, V. Barone, B. Mennucci, G. A. Petersson, H. Nakatsuji, M. Caricato, X. Li, H. P. Hratchian, A. F. Izmaylov, J. Bloino, G. Zheng, J. L. Sonnenberg, M. Hada, M. Ehara, K. Toyota, R. Fukuda, J. Hasegawa, M. Ishida, T. Nakajima, Y. Honda, O. Kitao, H. Nakai, T. Vreven, J. A. Montgomery, Jr., J. E. Peralta, F. Ogliaro, M. Bearpark, J. J. Heyd, E. Brothers, K. N. Kudin, V. N. Staroverov, R. Kobayashi, J. Normand, K. Raghavachari, A. Rendell, J. C. Burant, S. S. Iyengar, J. Tomasi, M. Cossi, N. Rega, J. M. Millam, M. Klene, J. E. Knox, J. B. Cross, V. Bakken, C. Adamo, J. Jaramillo, R. Gomperts, R. E. Stratmann, O. Yazyev, A. J. Austin, R. Cammi, C. Pomelli, J. W. Ochterski, R. L. Martin, K. Morokuma, V. G. Zakrzewski, G. A. Voth, P. Salvador, J. J. Dannenberg, S. Dapprich, A. D. Daniels, Ö. Farkas, J. B. Foresman, J. V. Ortiz, J. Cioslowski, and D. J. Fox, Gaussian 09, revision C.01; Gaussian Inc.: Wallingford, CT. 2009.
22. A. Daina, O. Michielin, and V. Zoete, *Scientific Reports*, **7,** 42717(2017), https://doi.org/10.1038/srep42717.
23. J. Tixier, G. Dusserre, S. Rault-Doumax, J. Ollivier, and C. Bourely, *Environmental Modelling and Software*, **17(7),** 627(2002), https://doi.org/10.1016/S1364-8152(02)00025-7.
24. W. Forli, S. Halliday, R. Belew, and A. Olson. AutoDock Version 4.2. Citeseer. 2012.
25. BIOVIA DS. Discovery Studio Visualizer v21.1.0.20298. BIOVIA, Dassault Systèmes. 2005.
26. M. Abraham, B. Hess, D. van der Spoel, and E. Lindahl. The GROMACS development team, GROMACS user manual. Version 5.0.7. 2015
27. A. W. Sousa Da Silva and W. F. Vranken, *BMC Research Notes*, **5,** 367(2012), https://doi.org/10.1186/1756-0500-5-367.
28. Q. Ke, X. Gong, S. Liao, C. Duan, and L. Li, *Journal of Molecular Liquids*, **365,** 120116(2022), https://doi.org/10.1016/j.molliq.2022.120116.
29. G. Poli, C. Granchi, F. Rizzolio, and T. Tuccinardi, *Molecules*, **25(8),** 1971(2020), https://doi.org/10.3390/molecules25081971.
30. L. Sun, Q. Lei, B. Peng, G. M. Kontogeorgis, and X. Liang, *Fluid Phase Equilibria*, **556,** 113398(2022), https://doi.org/10.1016/j.fluid.2022.113398.
31. G. Wang, *Journal of Biological Chemistry*, **283(47),** 32637(2008), https://doi.org/10.1074/jbc.M805533200.
32. D. Schneidman-Duhovny, Y. Inbar, R. Nussinov, and H. J. Wolfson, *Nucleic Acid Research*, **33(Issue suppl_2),** W363–W367(2005), https://doi.org/10.1093/nar/gki481.
33. A. Elengoe, M. Abu Naser, and S. Hamdan, *International Journal of Molecular Sciences*, **15(4),** 6797(2014), https://doi.org/10.3390/ijms15046797.
34. M. M. Damayanti, M. Rachmawati, E. Widiyastuti, Y. Kharisma, T. M. Fakih, A. Arfan and D.S.F. Ramadhan, *Rasayan Journal of Chemistry*, **Special Issue,** 158(2022), http://doi.org/10.31788/RJC.2022.1558192.
35. G. A. Gyebi, O. B. Ogunro, A. P. Adegunloye, O. M. Ogunyemi, and S. O. Afolabi, *Journal of Biomolecular Structure and Dynamics*, **39(9),** 3396(2020),

https://doi.org/10.1080/07391102.2020.1764868.
36. T. K. Karami, S. Hailu, S. Feng, R. Graham, and H. J. Gukasyan, *Journal of Ocular Pharmacology and Therapeutics*, **38(1),** 43(2022), https://doi.org/10.1089/jop.2021.0069.
37. Nurisyah, D. S. F. Ramadhan, R. Dewi, A. Asikin, D. R. Daswi, A. Adam, Chaerunnimah, Sunarto, Rafika, Artati, and T. M. Fakih, *Current Research in Structural Biology*, **7,** 100125(2024), https://doi.org/10.1016/j.crstbi.2024.100125.
38. M. F. R. Syaban, I. F. D. Faratisha, K. C. Yunita, N. E. Erwan, D. B. Kurniawan, and G. F. A. Putra, *Journal of Tropical Life Science*, **12(2),** 219(2022), https://doi.org/10.11594/jtls.12.02.08.
39. T. A. Yuniarta, I. G. A. Sumartha, T. M. Fakih, R. Handayani, and D. S. F. Ramadhan, *Jordan Journal of Pharmaceutical Sciences*, **16(4),** 880(2023), https://doi.org/10.35516/jjps.v16i4.1027.
40. F. K. Malik, and J. Guo, *Proteins*, **90(6)**, 1303(2022), https://doi.org/10.1002/prot.26313.
41. J. Vucinic, G. Novikov, C. Y. Montanier, C. Dumon, T. Schiex, and S. Barbe, *International Journal of Molecular Sciences*, **22(11)**, 5961(2021), https://doi.org/10.3390/ijms22115961.
42. K. Premavathi, P. Valentina, and N. Ramalakshmi, *Rasayan Journal of Chemistry*, **16(1)**, 227(2023), http://doi.org/10.31788/RJC.2023.1616995.
43. D. A. E. Pitaloka, D. S. F. Ramadhan, Arfan, L. Chaidir, and T. M. Fakih, *Scientia Pharmaceutica*, **89(2)**, 20(2021), https://doi.org/10.3390/scipharm89020020.
44. S. Ahmad, H. W. Abbasi, S. Shahid, S. Gul, and S. W. Abbasi, *Journal of Biomolecular Structure and Dynamics*, **39(12)**, 4225(2021), https://doi.org/10.1080/07391102.2020.17751295.
45. A. B. Coda, T. Hata, J. Miller, D. Audish, P. Kotol, A. Two, F. Shafiq, K. Yamasaki, J. C. Harper, J. Q. Del Rosso, and R. L. Gallo, *Journal of the American Academy of Dermatology*, **69(4)**, 570(2013), https://doi.org/10.1016/j.jaad.2013.05.019.
46. E. F. Ariyanto, W. A. Shalannandia, U. A. Lantika, T. M. Fakih, D. S. F. Ramadhan, A. N. Gumilar, F. K. Permana, A. N. Rahmah, N. Atik, and A. F. Khairani, *Journal of Experimental Pharmacology*, **15**, 217(2023), https://doi.org/10.2147/JEP.S405433.

[RJC- 8898/2024]